# Guided self-assembly of electrostatic binary monolayers via isothermal-isobaric control

Nickolay V. Shestopalov, Graeme Henkelman,[a] and Gregory J. Rodin[a]
*Institute for Computational Engineering and Sciences, The University of Texas at Austin, Austin, Texas 78712, USA*

(Received 11 November 2010; accepted 20 September 2011; published online 17 October 2011)

Self-assembly of a binary monolayer of charged particles is modeled using molecular dynamics and statistical mechanics. The equilibrium phase diagram for the system has three distinct phases: an ionic crystal; a geometrically ordered crystal with disordered charges; and a fluid. We show that self-assembly occurs near the phase transition between the ionic crystal and the fluid, and that the rate of ordering is sensitive to the applied pressure. By assuming an Arrhenius form for the rate of ordering, an optimality condition for the temperature and pressure is derived that maximizes the rate. Using the Clausius-Clapeyron equation, the optimal point on the phase boundary is expressed in terms of the thermodynamic changes in state variables across the boundary. The predicted optimal temperature and pressure conditions are in good agreement with numerical simulations and result in self-organization rates five times that of a simulation without applied pressure. © *2011 American Institute of Physics*. [doi:10.1063/1.3650370]

## I. INTRODUCTION

Self-assembly is a process that transforms a system of multiple components from a disordered to an ordered state. Self-assembly is ubiquitous to many natural phenomena, and it is of great technological importance, particularly in nanoscale manufacturing. Invariably, self-assembly involves a delicate balance between the global order and the local disorder; the latter is essential for removing local defects. The task of attaining and maintaining this delicate balance is challenging, and it can significantly benefit from guided as opposed to spontaneous self-assembly. Experimentally, the strength of this approach has been demonstrated for colloidal suspensions,[1,2] block copolymers,[3] and protein solutions.[4]

In this paper, motivated by experiments of Grzybowski *et al.*,[6] we consider self-assembly of electrostatic binary monolayers guided by the isothermal-isobaric control. Electrostatic binary monolayers represent rather simple systems, but this choice ideally fits our principal objective of developing a fundamental understanding of how to guide the self-assembly. This work builds on our previous work[5] on guided self-assembly of binary charged monolayers. In our previous work, we used temperature as a single control parameter and attempted to develop an optimal annealing schedule.[5] That study lead to two main conclusions. First, we determined that self-assembly did not benefit significantly from optimal time-dependent thermal control, when compared to a properly chosen isothermal control. Therefore, in this work, we adopt isothermal control. Second, we determined that thermal control was invariably inefficient in eliminating voids whose size was comparable to that of the particles. To address this issue, in this work, we utilize pressure as an additional control parameter, as it is ideally suited for closing voids. Indeed, we show that self-assembly of highly ordered structures is possible under properly chosen isothermal-isobaric conditions. Furthermore, we identify optimal conditions which result in rapid self-assembly, proceeding at a much faster rate than thermally guided self-assembly.

The paper is organized as follows. In Sec. II, we introduce the model system. In Sec. III, we develop the phase diagram. In Sec. IV, we identify optimal isothermal-isobaric conditions for rapid self-assembly. In Sec. V, we present a simplified thermodynamic model for determining optimal isothermal-isobaric conditions for guiding self-assembly. In Sec. VI, we summarize key results and discuss directions for further research.

## II. MODEL SYSTEM

As in our previous work,[5] the model system was chosen to represent experiments carried out by Grzybowski *et al.*[6] In those experiments, a horizontal tray of oppositely charged millimeter-size spherical particles was subjected to in-plane mechanical vibrations. Grzybowski *et al.* demonstrated that certain vibration programs would make the particles assemble into two-dimensional (2D) crystalline structures.

In this study, we considered binary monolayers formed by $3n$ charged spherical particles. The particles were divided into two groups: (i) $2n$ particles carried a charge $q$ each, and (ii) $n$ particles carried a charge $-2q$ each. In all other respects the particles were identical. For large $n$, a perfectly ordered state for such a system is a hexagonal lattice in which each negatively charged sphere is in contact with six positively charged spheres, and each positively charged sphere is in contact with three negatively charged spheres. The particles were placed in a square container which was treated as a unit cell of a periodic structure. Thus, the particles did not interact with

[a]Authors to whom correspondence should be addressed. Electronic mail: henkelman@mail.utexas.edu and gjr@ices.utexas.edu.

 

the container walls, but rather were allowed to penetrate them and reappear on the opposite side.

Although model systems considered by Grzybowski *et al*. should be treated as macroscopic and described using classical mechanics, we treated our systems as microscopic and relied on statistical mechanics. This choice was made to avoid difficulties associated with modeling and simulation of friction and contact. Accordingly, the system was agitated via thermal rather than mechanical vibrations. In addition, for better control, the system was subjected to external pressure. In all cases, the system was subjected to isothermal-isobaric conditions. The pressure was applied by varying the container size.

Electrostatic particle interactions were governed by basic Coulomb's law, so that the system's internal energy was computed via pairwise summation

$$U = \sum_{i,j<i} \frac{q_i q_j}{\epsilon_0 r_{ij}} + U_{rep}, \tag{1}$$

where $q$'s are the charges, $r$ is the inter-particle distance, and $\epsilon_0$ is the vacuum permittivity. The repulsive term,

$$U_{rep} = \gamma \frac{q^2}{\epsilon_0 d}\left[1 + \cos\left(\frac{\pi r_{ij}}{d}\right)\right], \tag{2}$$

was added to any pair of particles whose centers were closer than the particle diameter $d$: $r_{ij} < d$. A large constant $\gamma$ was introduced to penalize particle interpenetration, and as a result the particles were treated as slightly compressible; we verified that $\gamma = 100$ was sufficiently large.

The long-range electrostatic interactions were computed using Ewald's summation method.[7] In particular, we used 3D Ewald method with a special choice of parameters suited for computing 2D rather than 3D lattice sums.[8] Accordingly, the 3D cell was chosen as a cuboid $H \times L \times L$, rather than a square $L \times L$. The edge in the direction perpendicular to the monolayer plane was chosen $H = 3d$. This choice was sufficient for effectively turning-off inter-layer electrostatic interactions.

Throughout the paper, we use the particle diameter $d$ as the unit of length, the particle mass $m$ as the unit of mass, and $q^{-1}\sqrt{\epsilon_0 m d^3}$ as the unit of time. The chosen time unit is comparable to the period of vibrations of two particles near contact. The temperature $T$ was measured in the reduced units of energy alleviating the need for using Boltzmann's constant. All quantities of interest are defined as per particle averages.

## III. EQUILIBRIUM

Under isothermal-isobaric conditions, the system eventually reaches equilibrium. Thus, in identifying optimal conditions for ordering, we must first identify their range. After that we can identify optimal conditions leading to rapid kinetics. Accordingly, in this section, we construct a phase diagram of equilibrium states in the two-dimensional control space of temperature and pressure, $(T, P)$.

The phase diagram is shown in Fig. 1. It consists of three domains, each representing a phase. Those phases are as follows:

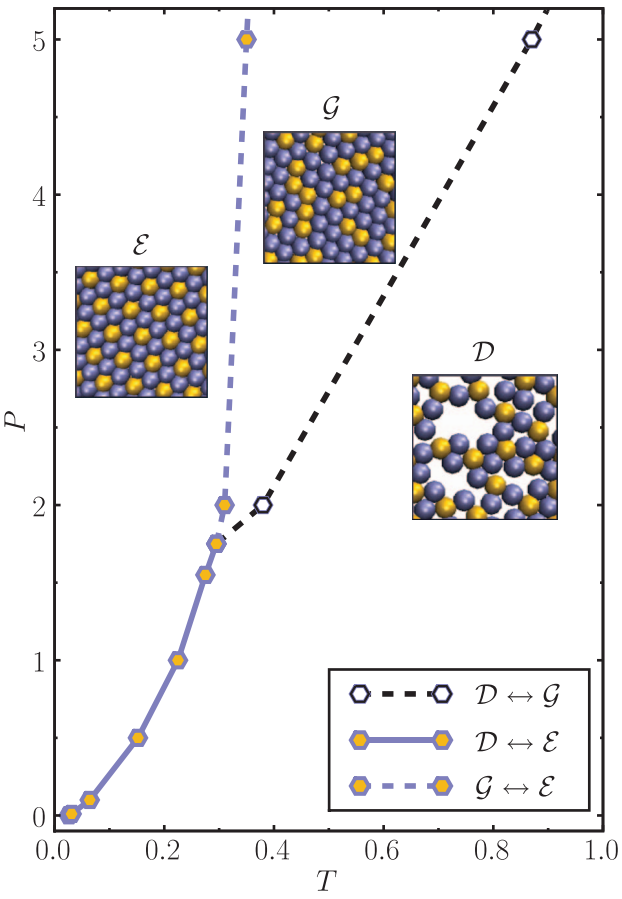


FIG. 1. The phase diagram of the system.

- disordered (fluid) phase ($\mathcal{D}$);
- geometrically but not electrostatically ordered phase ($\mathcal{G}$);
- geometrically and electrostatically ordered (ionic crystal) phase ($\mathcal{E}$).

Let us make it clear that the phase $\mathcal{E}$ does not necessarily have a perfect hexagonal structure. A small population of defects is not only possible but rather expected, as it is always the case with microscopic systems at non-zero temperature.

The phase diagram was constructed by computing points on the phase boundaries, shown by hexagonal symbols in Fig. 1. Those points were computed using the maximum fluctuations in the internal energy $U$,

$$\sigma_U = \frac{\sqrt{\langle U^2\rangle - \langle U\rangle^2}}{T} \tag{3}$$

and volume $V$,

$$\sigma_V = \sqrt{\frac{\langle V^2\rangle - \langle V\rangle^2}{VT}}, \tag{4}$$

where the angular brackets denote ensemble averaging.[15] To this end, we fixed $P$ and searched for the peaks of $\sigma_U$ and $\sigma_V$ by traversing the phase space along the $T$-axis. The phase boundaries were identified according to the following algorithm:[15]

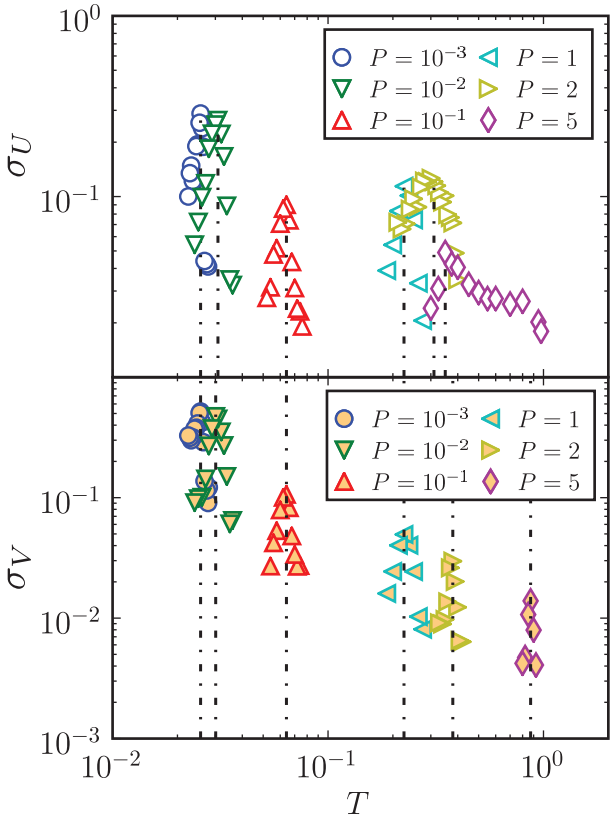


FIG. 2. Fluctuations in energy, $\sigma_U$, and volume, $\sigma_V$, as functions of temperature and pressure; peaks show locations of phase transitions.

- if a temperature $T$ realizes maxima of both $\sigma_U$ and $\sigma_V$, then the point $(T, P)$ is on the boundary between the phases $\mathcal{D}$ and $\mathcal{E}$;
- if a temperature $T$ realizes a maximum of $\sigma_U$ but not of $\sigma_V$, then the point $(T, P)$ is on the boundary between the phases $\mathcal{G}$ and $\mathcal{E}$;
- if a temperature $T$ realizes a maximum of $\sigma_V$ but not of $\sigma_U$, then the point $(T, P)$ is on the boundary between the phases $\mathcal{D}$ and $\mathcal{G}$.

This algorithm is self-explanatory once it is realized that the transition between $\mathcal{G}$ and $\mathcal{E}$ is associated with essentially constant volume, and the transition between $\mathcal{G}$ and $\mathcal{D}$ is associated with minimal changes in the internal energy. The peaks of $\sigma_U$ and $\sigma_V$ for a broad range of conditions are shown in Fig. 2.

For prescribed isothermal-isobaric conditions, the internal energy and volume were computed using replica exchange molecular dynamics (REMD) (Ref. 10) as implemented in the publicly available code LAMMPS.[11] Constant temperature and pressure of the system were maintained with a Nose-Hoover thermostat[12] and a Berendsen barostat,[13] respectively. Each replica consisted of 1020 particles. To improve the sampling at high pressures, we augmented REMD with additional Monte Carlo moves. Each move attempted to switch two oppositely charged particles. Both the particle and replica exchanges were based on the standard Metropolis acceptance criterion for an isothermal-isobaric statistical ensemble.[14] The maximum $\sigma_U$ and $\sigma_V$ were obtained by averaging over 100 realizations. Further, we verified that results shown in Fig. 2 were insensitive to particulars of the initial configurations.

Certain properties of the phase diagram can be readily explained using the Clausius-Clapeyron relationship for the phase boundary quantities:[9]

$$\frac{dP}{dT} = \frac{[[S]]}{[[V]]}\,. \tag{5}$$

Here, $[[...]]$ denotes the jump across the phase boundary and $S$ is the entropy.

Across the boundary $\mathcal{G} - \mathcal{E}$, $[[V]]$ is small. Therefore, this boundary is essentially a vertical line; the large but finite slope of this line is due to slight compressibility of the particles.

The phases $\mathcal{G}$ and $\mathcal{D}$ have different particle densities, but both are characterized by the absence of electrostatic order. Therefore, across the boundary $\mathcal{G} - \mathcal{D}$, the dominant contribution to $[[S]]$ is due to the difference in free volume:

$$[[S]] \propto \log V_{\mathcal{D}} - \log V_{\mathcal{G}} = \log\left(1 + \frac{[[V]]}{V_{\mathcal{G}}}\right); \tag{6}$$

here, the subscripts refer to the phases. At high pressures, $[[V]] \ll V_{\mathcal{G}}$, and therefore the right-hand side of Eq. (6) can be linearized, so that we obtain

$$\frac{[[S]]}{[[V]]} \propto \frac{1}{V_{\mathcal{G}}}\,. \tag{7}$$

Since the particles are virtually incompressible ($\gamma \gg 1$), $V_{\mathcal{G}}$ is essentially constant, and therefore, for large $P$, the boundary between the phases $\mathcal{G}$ and $\mathcal{D}$ is also a straight line.

## IV. KINETICS

In this section, we are concerned with kinetics of transition to the phase $\mathcal{E}$. Electrostatic order in the system was measured using the order parameter

$$\eta(t) = \frac{\hat{U}(0) - \hat{U}(t)}{\hat{U}(0) - \Psi}\,, \tag{8}$$

where the hat refers to the inherent as opposed to the instantaneous structure. The inherent structure is obtained upon quenching of the instantaneous configuration under constant pressure. The inherent structure concept was introduced by Stillinger and Weber[16] and we adopted it because it allowed us to evaluate structural regularity at different points of the phase diagram. In Eq. (8), $t$ denotes time and $\Psi$ denotes the internal energy of the perfect hexagonal lattice. The order parameter $\eta$ is small in the disordered phase and equal to one for a perfect hexagonal lattice. The constant pressure associated with the inherent structure may differ from the applied one. In comparing the histories $\eta(t)$ under different isothermal-isobaric conditions, we consider intrinsic structures at zero pressure. In contrast, in studying microstructural evolution under fixed isothermal-isobaric conditions, it is more natural to consider intrinsic structures by maintaining the applied pressure.

Figure 3 shows the data $\eta(t)$ for several points $(T, P)$ located inside the phase $\mathcal{E}$ on the phase diagram; the chosen points are shown in the figure inset. Conditions outside of

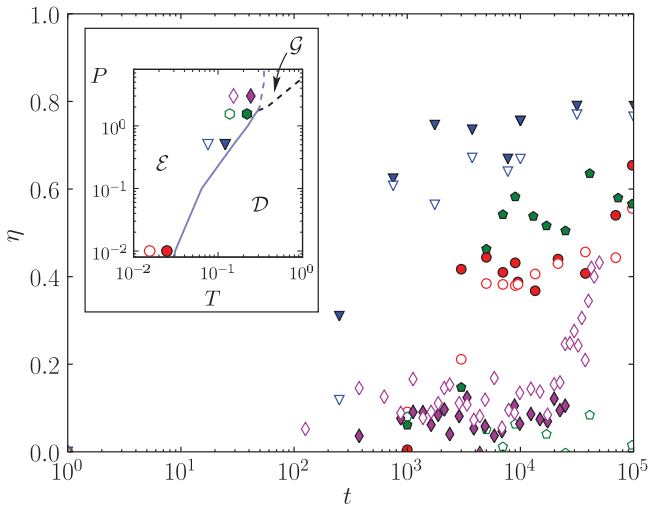


FIG. 3. Order parameter $\eta$ as a function of time for selected $T$ and $P$.

the phase $\mathcal{E}$ would not lead to ordering and were not considered. The histories corresponding to the points located near the phase boundary are shown using closed symbols, while the points at lower temperatures, away from the phase boundaries, with open symbols. Among the points near the boundary, the fastest approach $\eta \to 1$ corresponds to the point below the triple-point junction; in Fig. 3 this history is shown with triangular symbols.

Numerical results presented here were obtained using MD. All simulations were conducted with 1020 particles whose initial positions represented a disordered state, determined by equilibrating the system at $T = 1$ and $P = 0.4$. It was established that details of the initial state were insignificant as long as it was well inside the phase $\mathcal{D}$ on the phase diagram. Furthermore, the simulations were repeated with 2340 particles and it was verified that the two sets of results were in agreement.

A better understanding of the ordering mechanism comes from examining microstructural evolution. To this end we studied the system of 2340 particles. As seen in the left column of Fig. 4, in the low-pressure regime (circular symbols in Fig. 3), ordering is slowed by system's inability to close inter-cluster voids. In contrast, as seen in the right column of Fig. 4, in the high-pressure regime (hexagonal and diamond-shaped symbols in Fig. 3), ordering is slowed by insufficient volume available for electrostatic reordering. Inherent structures shown in Fig. 4 were quenched at the simulation pressure.

Figure 5 shows evolving microstructures under optimal isothermal-isobaric conditions (closed triangles in Fig. 3). Here, we use the term optimal rather loosely, by referring to the best conditions for ordering among the limited set of conditions chosen for simulations. The left and right columns of Fig. 5 show the instantaneous and intrinsic microstructures, respectively. Visually, optimality can be associated with a competitive balance between vacancies (low-pressure defects) and electrostatic irregularities (high-pressure defects). In comparing optimal versus non-optimal conditions and microstructures, it is important to keep in mind that the total

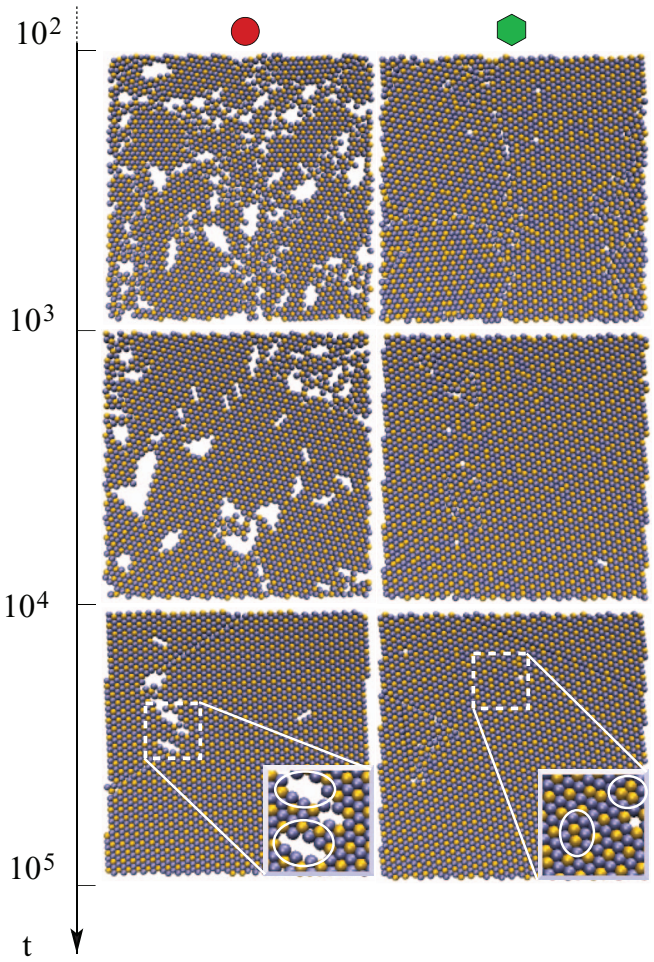


FIG. 4. Evolving microstructures under low (left column) and high (right column) pressures.

simulation time for the former (Fig. 5) is roughly one order of magnitude shorter than that for the latter (Fig. 4).

Simulation results for the points away from the boundary (open symbols in Fig. 3) demonstrate that an optimal $(T, P)$ point should be close to the phase boundary. In general though, the issue of proximity to the phase boundary is a delicate one. In the present context, it is further complicated by the fact that the phase boundaries have finite width $\delta T$ due to the finite system size. We selected the points near the boundary by shifting them by $0.1\,T^*$ to the left from the boundary, where $T^*$ is the transition temperature on the boundary of $\mathcal{E}$. In all cases, this shift was larger than $\delta T/2$, so that the isothermal-isobaric conditions were located inside the domain of phase $\mathcal{E}$.

## V. THERMODYNAMIC MODEL FOR OPTIMAL CONDITIONS

In this section, we present a basic thermodynamic model that allows us to establish explicit relationships between kinetic and equilibrium properties and to obtain a simple mathematical expression for the optimal conditions.

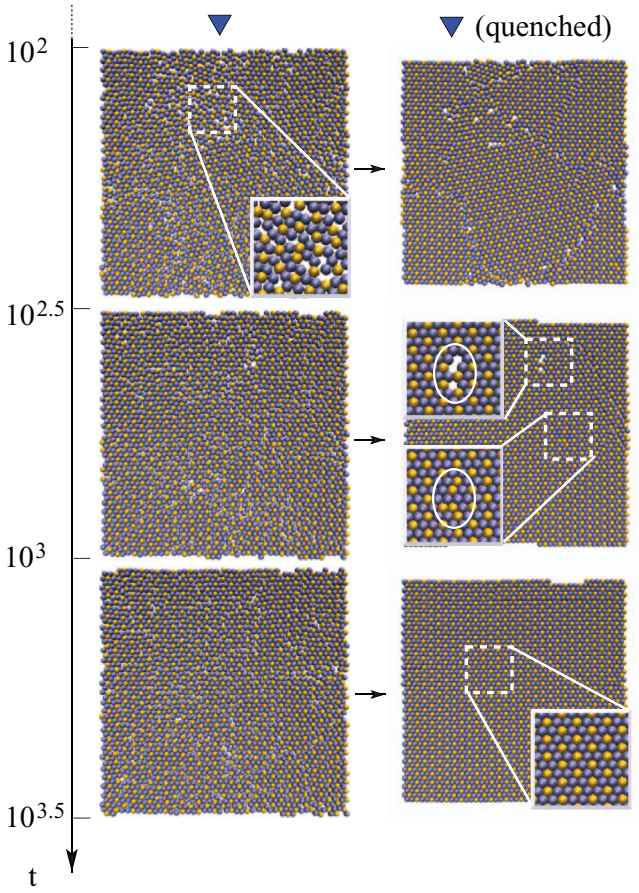


FIG. 5. Evolving microstructures under optimal pressure.

Suppose that the optimal point $(T_0, P_0)$ belongs to a curve $P = \psi(T)$, so that $T_0$ can be found from the equation

$$\frac{\partial k}{\partial T} + \frac{\partial k}{\partial P}\,\frac{\mathrm{d}\psi(T)}{\mathrm{d}T} = 0, \tag{9}$$

where $k$ is the rate of ordering; once $T_0$ has been determined, one obtains $P_0 = \psi(T_0)$.

Assume that the transition between the phases $\mathcal{D}$ and $\mathcal{E}$ is governed by a mechanism whose rate obeys the exponential law for state transitions:[17]

$$k = \nu \exp\left(-\frac{\Delta G(T, P)}{T}\right). \tag{10}$$

Here, $\nu$ is a constant characteristic frequency and $\Delta G$ is the activation free energy barrier between the states. By combining Eqs. (9) and (10) we obtain

$$\Delta G - T\,\frac{\partial \Delta G}{\partial T} = T\,\frac{\partial \Delta G}{\partial P}\,\psi'. \tag{11}$$

Let us rewrite this equation using the following definitions:

$$\Delta V := \frac{\partial \Delta G}{\partial P}$$

and

$$\Delta U := \Delta G - T\frac{\partial \Delta G}{\partial T} - P\frac{\partial \Delta G}{\partial P},$$

so that Eq. (11) takes the form

$$\frac{\Delta U}{\Delta V} + \psi(T) = T\psi'(T). \tag{12}$$

Based on simulation results presented in Sec. IV, we assume that the curve $\psi$ is the boundary between the phase domains $\mathcal{D}$ and $\mathcal{E}$. On the surface, this is a bad assumption because $(T_0, P_0)$ must be inside the phases $\mathcal{E}$. Nevertheless, our intent is to adopt the assumption and determine the point $(T^*, P^*)$ on the phase boundary, and then determine the optimal point as $(T_0, P_0) = (0.9T^*, P^*)$, by using the shift discussed in Sec. IV. With the assumption that $\psi$ is the boundary, Eq. (12) can be combined with Clausius-Clapeyron equation (5) to obtain the optimality condition in the form

$$\frac{\Delta U}{\Delta V} = \frac{[[U]]}{[[V]]}. \tag{13}$$

The right-hand side of Eq. (13) can be approximately evaluated using Lindemann's melting criterion. According to that criterion, melting occurs when the average inter-particle distance increases by a factor of $1 + \alpha$, where $\alpha$ is a small constant; following Ref. 18 we set $\alpha = 1/7$. The increase in inter-particle separation is associated with the changes in the activation internal energy and volume, estimated as

$$\Delta U = \left(\frac{1}{1+\alpha} - 1\right)\Psi$$

and

$$\Delta V = \frac{\sqrt{3}}{2}[(1+\alpha)^2 - 1],$$

respectively. With these estimates, Eq. (13) becomes

$$\frac{[[U]]}{[[V]]} = 0.36.... \tag{14}$$

We solved this equation for the data used for constructing the boundary between the phases $\mathcal{D}$ and $\mathcal{E}$ and obtained the optimal point $(T_0, P_0) = (0.1, 0.3)$.

To verify this estimate for the optimal point we conducted MD simulations using the following three-step procedure:

- Select a point $(T^*, P^*)$ on the boundary between the phases $\mathcal{D}$ and $\mathcal{E}$.
- Equilibrate the system under the conditions $(1.1T^*, P^*)$ and use that state as the initial one.
- Let the initial state evolve for 4000 time units under the conditions $(0.9T^*, P^*)$.

The ordering rate $k$ for prescribed $(T^*, P^*)$ $k$ was obtained by computing the best fit to the equation

$$\eta = 1 - \exp(-kt), \tag{15}$$

where $\eta$ is the order parameter defined in Eq. (8).

Figure 6 shows the transition rate for various pairs $(T^*, P^*)$ along the phase boundary between the phases $\mathcal{D}$ and $\mathcal{E}$. The circles represent the points on the boundary and the crosses represent the points $(0.9T^*, P^*)$; the numbers are the corresponding transition rates per $10^4$ time units. The square denotes the optimal point predicted by the simplified model.

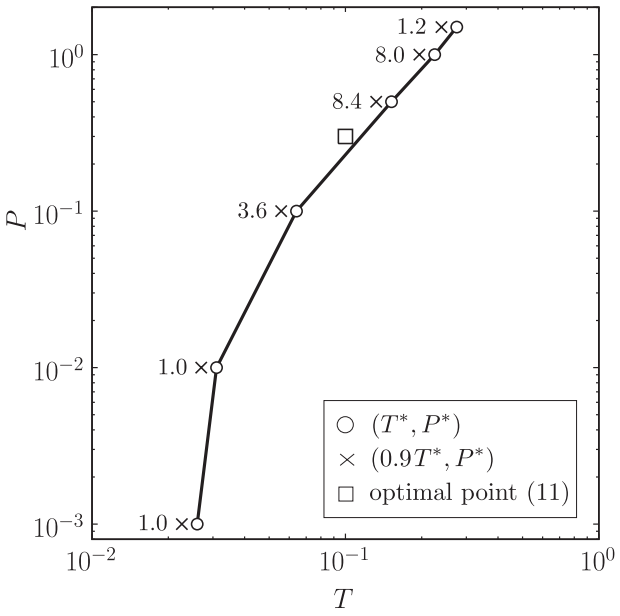


FIG. 6. Average ordering rate for various pairs ($T^*$, $P^*$) along the phase boundary between the phases $\mathcal{D}$ and $\mathcal{E}$.

Considering the assumptions involved in deriving Eq. (14), its prediction for the optimal point is quite good.

## VI. DISCUSSION

This paper is concerned with controlling self-assembly in binary monolayers of charged particles. The paper was motivated by experiments carried out by Whitesides *et al.*[6] on controlling macroscopic self-assembly, and by our previous work,[5] on modeling and simulation of thermally controlled microscopic self-assembly. In particular, in our previous work, we observed that (i) isothermal control can be almost effective as optimal time-dependent thermal control, and (ii) neither electrostatic interactions nor thermal control were particularly effective in eliminating voids formed during self-assembly. Accordingly, this paper focuses on the temperature-pressure control under isothermal-isobaric conditions.

From our simulations, we determined that optimal isothermal-isobaric control is up to five times more effective than thermal control alone. This statement is based on comparing the histories for the order parameter $\eta$ defined in Eq. (8) and microstructures shown in Figs. 4 and 5. While isothermal-isobaric control is capable of delivering microstructures with low defectivity, those microstructures are not perfect, and should not be expected to be perfect, simply because microscopic systems are intrinsically imperfect at non-zero temperatures. Of course, there are no fundamental reasons against realizing perfect macroscopic structures. In this regard, let us mention that isothermal-isobaric control is ineffective for eliminating defects such as dislocation and twins. Signatures of those defects can be seen in microstructures under high-pressure conditions (Fig. 4), and, as basic crystal physics suggests, those defects are expected to persist as the system size increases. The natural control for eliminating those dislocation and twins is shearing the system.

In identifying optimal temperature and pressure conditions, we adopted several assumptions that allowed us to relate those conditions to the phase diagram. Instead of verifying the individual assumptions, we verified the approximation itself, and determined that it agrees well with MD simulations. Some discussion of Eq. (13) is warranted. For the sake of argument, both sides of Eq. (13) can be divided by $P$,

$$\frac{[[U]]}{P[[V]]} = \frac{\Delta U}{P\Delta V}. \tag{16}$$

In this form, the right-hand side of the equation is the non-dimensional ratio of the energy to the mechanical work required for ordering at some pressure $P$. The left-hand side is the non-dimensional ratio of the change in internal energy to the associated mechanical work due to the phase change. In general, there is no reason to assume a simple relationship between the kinetic parameters $\Delta U$ and $\Delta V$ and the equilibrium changes across the phase transition $[[U]]$ and $[[V]]$. Equation (16), however, serves the purpose of identifying the point on the phase boundary with the optimal balance between $T$ and $P$. At this point the effect of accelerating the kinetics by increasing the temperature exactly matches the resulting penalty in terms of the mechanical work.

## ACKNOWLEDGMENTS

Funding for G. J. R. was provided by the Department of Energy (Grant No. DE-FG02-05ER25701) and for G. H. by the National Science Foundation (Grant No. CHE 0645497). Both were supported by the W. A. "Tex" Moncrief, Jr., Endowment In Simulation-Based Engineering Sciences through Grand Challenge Faculty Fellowships from the Institute of Computational and Engineering Sciences at The University of Texas at Austin. N. V. S. was supported by a Fellowship in Computational and Applied Mathematics from the Institute of Computational and Engineering Sciences at The University of Texas at Austin. Computational resources were provided by the Texas Advanced Computing Center.

[1] F. Nadal, F. Argoul, P. Hanusse, B. Pouligny, and A. Ajdari, Phys. Rev. E **65**, 061409 (2002).
[2] A. Yethiraj, Soft Matter **3**, 1099 (2007).
[3] A. C. Edrington, A. M. Urbas, P. DeRege, C. X. Chen, T. M. Swager, N. Hadjichristidis, M. Xenidou, L. J. Fetters, J. D. Joannopoulos, Y. Fink, and E. L. Thomas, Adv. Mater. **13**, 421 (2001).
[4] A. Stradner, H. Sedgwick, F. Cardinaux, W. C.K. Poon, S. U. Egelhaaf, and P. Schurtenberger, Nature (London) **432**, 492 (2004).
[5] N. V. Shestopalov, G. Henkelman, C. T. Powell, and G. J. Rodin, New J. Phys. **11**, 053014 (2009).
[6] B. A. Grzybowski, A. Winkelman, J. A. Wiles, Y. Brumer, and G. M. Whitesides, Nature Mater. **2**, 241 (2003).
[7] P. J. in't Veld, A. E. Ismail, and G. S. Grest, J. Chem. Phys. **127**, 144711 (2007).
[8] Yeh and Berkowitz, J. Chem. Phys. **111**, 3155 (1999).
[9] D. A. McQuarrie, *Statistical Thermodynamics* (Harper & Row, New York, 1973).
[10] A. Mitsutake, Y. Sugita, and Y. Okamoto, Biopolymers **60**, 96 (2001).

[11]S. Plimpton, J. Comput. Phys. **117**, 1 (1995).
[12]G. J. Martyna, M. E. Tuckerman, D. J. Tobias, and M. L. Klein, Mol. Phys. **87**, 1117 (1996).
[13]H. J.C. Berendsen, J. P.M. Postma, W. F. Vangunsteren, A. Dinola, and J. R. Haak, J. Chem. Phys. **81**, 3684 (1984).
[14]D. Frenkel and B. Smit, *Understanding Molecular Simulation* (Academic, New York, 2002).
[15]M. R. Manaa, *Chemistry at Extreme Conditions* (Elsevier, New York, 2005).
[16]F. H. Stillinger and T. A. Weber, Science **225**, 983 (1984).
[17]S. Glasstone, K. J. Laidler, and H. Eyring, *The Theory of Rate Processes* (McGraw-Hill, New York/London, 1941).
[18]D. Tabor, *Gases, Liquids, and Solids* (Cambridge University Press, Cambridge, England, 1979).